Comparison of Decoupling Methods for Analyzing Pressure Fluctuations in Gas-Fluidized Beds

Yongmin Zhang
State Key Laboratory of Heavy Oil Processing, China University of Petroleum, Beijing 102249, P.R. China

Hsiaotao T. Bi and John R. Grace
Fluidization Research Centre, Dept. of Chemical and Biological Engineering, University of British Columbia, Vancouver, BC V6T 1Z3, Canada

Chunxi Lu
State Key Laboratory of Heavy Oil Processing, China University of Petroleum, Beijing 102249, P.R. China

DOI 10.1002/aic.12052
Published online October 20, 2009 in Wiley InterScience (www.interscience.wiley.com).

Two methods of decoupling pressure fluctuations in fluidized beds by using the incoherent part (IOP) of absolute pressure (AP) and differential pressure (DP) fluctuations are evaluated in this study. Analysis is conducted first to demonstrate their similarities, differences, and drawbacks. Then, amplitudes, power spectral densities, mean frequencies, coherence functions, and filtering indices of the IOP of AP and DP fluctuations are calculated and compared based on experimental data from a two-dimensional fluidized column of FCC particles. Derived bubble sizes are also compared with the sizes of bubbles viewed in the two-dimensional bed. The results demonstrate the similarity of these two methods in filtering out global compression wave components from absolute pressure fluctuations, especially those generated from oscillations of fluidized particles and gas flow rate fluctuations. However, both methods are imperfect. Neither can filter out all the compression wave components and retain all the useful bubble-related wave components. Their amplitudes can be used to characterize global bubble property and quality of gas–solids contacting in bed, but they do not give accurate measurement of bubble sizes. © 2009 American Institute of Chemical Engineers *AIChE J,* 56: 869–877, 2010
Keywords: pressure fluctuations, fluidized bed, decoupling, diagnostics

Introduction

Fluidized beds are widely used in various physical and chemical applications. Pressure fluctuations have long provided qualitative information on the dynamics of gas–solids-fluidized beds. In recent years, considerable attention has been devoted to the study of pressure fluctuations to understand their origin and interpret their nature in terms of the complex hydrodynamics.

In typical bubbling fluidized beds, pressure fluctuations arise from a combination of local pressure variations induced by bubble passages and remote compression waves, with the latter originating from a number of hydrodynamic phenomena, such as generation, coalescence, break-up, and eruption of bubbles, as well as gas flow rate fluctuations.[1,2] Decoupling the pressure signals in fluidized beds is very attractive, as it can be an effective means, for example, of estimating the average bubble size in a fluidized bed. From the bubble

Correspondence concerning this article should be addressed to H. T. Bi at xbi@chml.ubc.ca

model of Davidson,[3] the amplitude of bubble-passage-induced pressure waves is proportional to the bubble diameter. Therefore, if remote compression pressure waves can be selectively removed from a pressure signal, the remainder of the signal should enable quantification of the average diameter of the passing bubbles, a crucial parameter determining the quality of gas–solids contacting in fluidized beds and the performance of fluidized-bed reactors. As pressure fluctuations are easily measured, even in high-temperature industrial-scale units, these methods are potentially very useful, especially in harsh environments where other measurement techniques are impossible.

Two alternative decoupling methods have shown good potential for some experimental conditions and have received certain recognition in the fluidization community. One, proposed by van der Schaaf et al.,[4] separated the power spectral density (PSD) of absolute pressure (AP) signals into a coherent part (COP) and an incoherent part (IOP) by a frequency-domain-based coherence function. This coherence function is calculated from two pressure signals: $p(x)$, measured in the plenum chamber below the gas distributor and $p(y)$, measured in the bed,

$$g_{xy}^2(f) = \frac{f_{xy}(f) f_{xy}^*(f)}{f_{xx}(f)_{yy}(f)}, \tag{1}$$

where ϕ_{xx} and ϕ_{yy} are the PSDs of the chamber and bed pressure signals, respectively, whereas ϕ_{xy} is their cross PSD and f_{xy}^* is the conjugate of ϕ_{xy}. The PSD of the bed pressure signal is then divided into a COP,

$$\mathrm{COP} = g_{xy}^2 f_{yy}, \tag{2}$$

and an IOP,

$$\mathrm{IOP} = \left(1 - g_{xy}^2\right) f_{yy}. \tag{3}$$

As local pressure waves generated in the bed are unlikely to be sensed in the plenum chamber, IOP is assumed to be composed only of local waves related to bubbles or gas turbulence.[4] The amplitude of IOP is then used to estimate the bubble size in fluidized beds of Geldart B particles by

$$d_b = \sigma_{xy,i} / \rho_p g (1 - \varepsilon_{mf}), \tag{4}$$

where $\sigma_{xy,i}$ is the standard deviation of IOP. The authors found that bubble sizes determined by Eq. 4 were in good agreement with those predicted by the semi-empirical equation of Darton et al.[5] Kleijn van Willigen et al.[6] applied this method to a two-dimensional fluidized bed with two types of particles: coarse sand (Geldart B) and fine glass beads (Geldart A). However, different scaling factors were needed to bring the bubble sizes inferred from Eq. 4 into alignment with experimental values measured by image analysis.

The other method is based on differential pressure (DP) fluctuations. Roy and Davidson[7] showed that the amplitude of DP fluctuations measured across a small axial interval inside a bubbling fluidized bed was proportional to the bubble size. Later, Bi[8] proved that compression wave components can be filtered out by a DP transducer with a small separation distance between its two taps, making differential signals more useful than absolute (single-port) pressure measurements.

These two decoupling methods have only been used so far in a limited number of laboratory-scale fluidized beds, with few types of particles examined. No study has been reported in which the two decoupling methods have been compared. In this study, we apply and compare the two decoupling methods in a two-dimensional fluidized bed, allowing bubble sizes to be roughly estimated from visual observation. This facilitates identification of the advantages and limitations of the two methods.

Theoretical Considerations

The two decoupling methods are based on different filtration principles. Decoupling by DP fluctuations is based on the different propagation velocities of compression waves and bubble-passage-induced waves. Bubble-passage-induced waves propagate at the same velocities as the bubble rise velocities, usually less than 2 m/s. On the other hand, the propagating velocity of compression wave is in the range of 5–30 m/s, with the higher limit ($\sim$30 m/s) for voidage close to minimum fluidization conditions and decreasing quickly to $\sim$10 m/s with bed voidage increasing to that at minimum bubbling.[9,10] Compression waves are also subject to serious attenuation in the presence of bubbles, especially in fluidized beds with high bubble volume fractions.[11] To filter out more compression wave components, the distance between the two taps of a DP transducer should be relatively small (same order as the bubble diameter). On the other hand, given the pressure field around a single bubble,[3] the distance should be no less than half a bubble diameter to minimize removal of bubble-passage-induced wave components. In most gas–solids-fluidized beds, bubbles are of a wide range of sizes, making it difficult to choose the most suitable spacing of the two taps of a DP transducer. This also means that it is likely to be impossible to avoid removal (filtering) of some bubble-passage-induced wave components, while some compression wave components also remain in processed DP signals.

The IOP method[4] is based on the degree of similarity in the frequency domain between a chamber pressure signal and a bed pressure signal. Components in a pressure signal measured in the bed with a frequency equal to the chamber pressure signal are selectively removed. The advantage of this decoupling method is that the attenuation because of the presence of bubbles no longer influences the filtering of compression wave components. However, it is also possible that the compression and bubble-passage-induced wave components overlap in their PSDs, leading to removal (filtering) of some bubble-passage-induced wave components. On the other hand, the gas distributor alters some components of compression waves, with the consequence that the chamber pressure signal cannot contain all the compression wave components in the bed. As a result, it is also difficult for the IOP method to completely separate the two types of pressure signals based on frequency domain analysis. In the data analysis later, we use a simple example to confirm this statement. Figure 1 plots the axial profiles of $\sigma_{xy;i}$, measured by van der Schaaf et al.[4] in an experimental column of 0.385

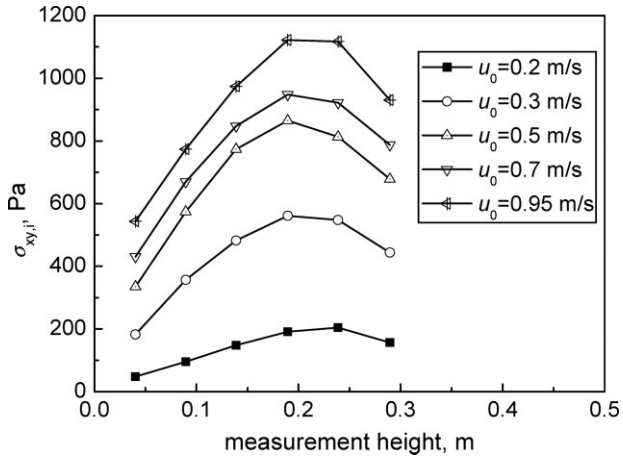

Figure 1. Standard deviation of incoherent pressure fluctuations ($\sigma_{xy,i}$) vs. measurement height in a bubbling fluidized bed for different gas velocities (sand: d_p = 0.38 mm, ρ_p = 2650 kg/m^3, d_t = 0.385 m, data obtained from van der Schaaf et al.[4]).

I.D., under different superficial gas velocities. For every superficial gas velocity, $\sigma_{xy;i}$ reached a peak in the upper part of the bed. If the bubble size is proportional to $\sigma_{xy;i}$, there should be a maximum bubble size in the upper part of the bed. This is inconsistent with previous experimental findings for both Geldart A and B particles[5,12–14] and also demonstrates that IOP is not composed of bubble-passage-induced-wave components.

In summary, both decoupling methods have drawbacks in analyzing pressure fluctuations for characterizing bubble properties. In the following sections, we analyze and compare these two methods based on our experimental measurements to verify these conclusions and to provide further comparison with experimental data.

Experimental Set-Up and Measurement Techniques

A schematic of the experimental set-up appears in Figure 2. The main column, with a cross-section of 500 mm × 30 mm and a height of 6 m, was constructed of plexiglass. This ''two-dimensional'' design provided direct views of the flow behavior of gas and solids. Although unsteady motion and distribution of the small bubbles generated by frequent splitting and coalescence in the fluidized bed of FCC particles prevented accurate measurement of bubble sizes by image analysis, the approximate bubble sizes and the quality of gas–solids contacting could be estimated roughly by visual observations. The column consisted of six sections of height 1 m, connected by flanges. The gas distributor was an 11-hole perforated plate with a 1.44% open area. Two-stage external cyclones captured particles entrained in the discharge gas flow and returned them to the dense bed via standpipes to maintain a constant solids inventory in the column.

Ambient air was introduced by a Roots blower. Equilibrium FCC particles of mean diameter 78 μm and density of 1500 kg/m^3 were the bed solids. The static bed height was maintained at 1.28 m for all experiments. The superficial gas velocity ranged from 0.2 to 1.1 m/s, covering both the bubbling and turbulent flow regimes.

Three pressure taps were installed flush with the inner wall of the column, two in the dense bed, 0.11 m (P_1) and 0.31 m (P_2) above the distributor, respectively, and the other in the plenum chamber (P_0). Each pressure tap was a steel tube of 7 mm ID. Wire gauze was inserted into the tip of each pressure tap to prevent entry or blockage by fine particles. The dead volume of each pressure measurement system was less than 8000 mm^3 throughout this study, which has been shown to give negligible damping of fluidized-bed pressure signals.[15] Three AP pressure transducers were used to obtain the transient pressure signals from the three taps. With this measurement arrangement, the differential signal between P_1 and P_2 could also be obtained. Absolute pressure transducers in this study were Gems-1200. The analog signals from transducers were converted into digital signals by an ADLINK PCI9111-DG A/D converter and then saved in a computer. For measuring pressure fluctuations, the minimum sampling frequency is usually required to be greater than 20 Hz to satisfy the Nyquist Sampling Criterion.[1] The sampling frequency here was 200 Hz and the sampling interval was 60 s for all runs.

Experimental Results

Comparison of fluctuation amplitudes

Figure 3 compares the fluctuation amplitudes (represented by the standard deviations) of AP signals (P_1), its IOP and COPs with respect to the chamber pressure signals (P_0), and DP signals between the P_1 and P_2 bed pressure taps, represented by σ_p, $\sigma_{xy,i}$, $\sigma_{xy,c,}$ and $\sigma_{dp,}$ respectively. As the superficial gas velocity increased, all four standard deviations first

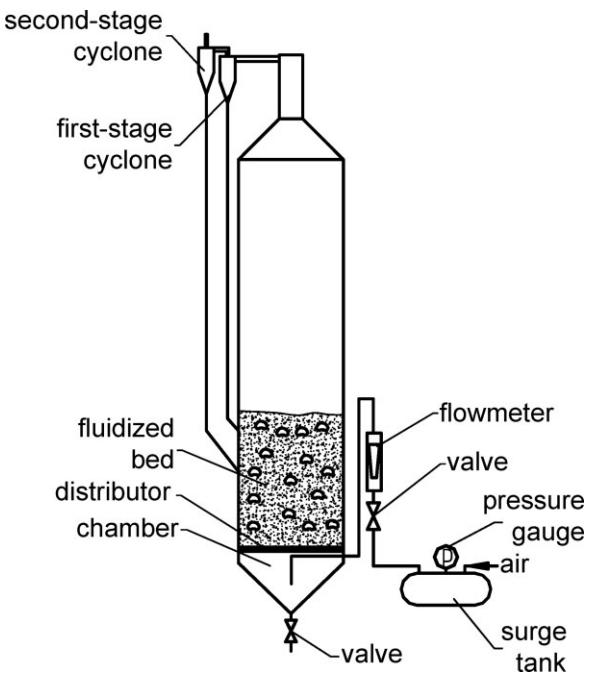

Figure 2. Schematic of two-dimensional experimental cold model column.

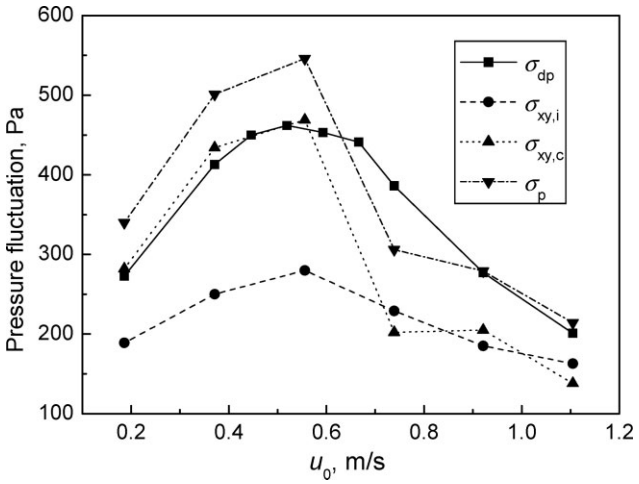

Figure 3. Comparison of amplitudes (represented by the standard deviation) of absolute pressure signals (σ_p), their incoherent and coherent parts ($\sigma_{xy,i}$ and $\sigma_{xy,c}$) with respect to the chamber pressure signals, and differential pressure signals (σ_{dp}).

increased, and then decreased after passing through a maximum at a superficial gas velocity approximately coinciding with the onset of turbulent flow regime. The σ_p and $\sigma_{xy,c}$ curves are similar in shape, indicating that the AP fluctuation signal is mainly composed of compression wave components. This is because the bubbles in fluidized beds of FCC particles are usually small, so the fluctuations caused by bubble-passage-induced waves are also small. The $\sigma_{xy,i}$ and σ_{dp} curves are similar in shape, but σ_{dp} is always larger than $\sigma_{xy,i}$. This is because local bubble-passage-induced waves constitute the main parts of both IOP and DP, so they follow similar trends with increasing superficial gas velocity. The difference in magnitude may arise from several causes. First, as shown in Figure 4, when the distance between the two taps of a DP transducer is large enough, the bubble-passage-induced components of the two AP signals become uncorrelated. Therefore, the DP signal may contain bubble-passage-induced components of the two AP signals. Second, there may still be significant compression wave components left in the DP signal, because the distance between the two taps of the DP transducer is not small enough.

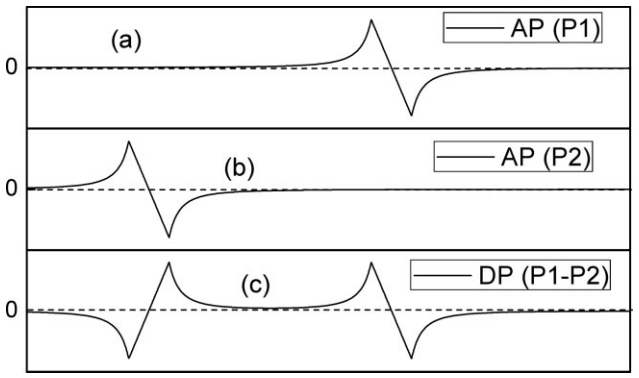

Figure 4. Absolute and differential pressure signals.

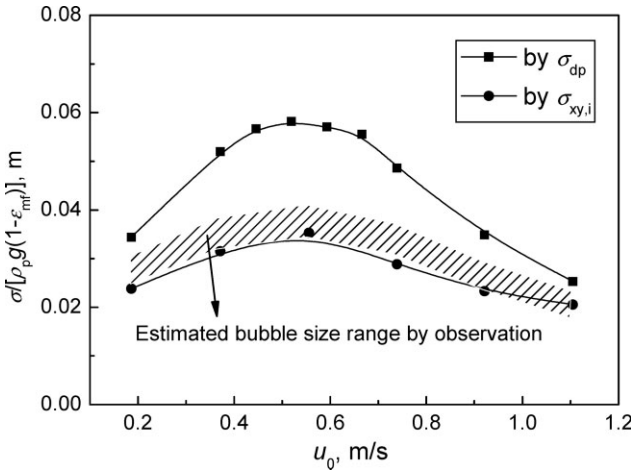

Figure 5. Estimated bubble sizes by differential pressure fluctuation and IOP.

The bubble size in the bed can be estimated from the amplitudes of the DP fluctuations and IOP by Eq. 4. Figure 5 plots and compares the two estimated bubble sizes as a function of superficial gas velocity. It is seen that bubble sizes estimated from $\sigma_{xy,i}$ ranged from 2 to 4 cm. Bubble sizes estimated from σ_{dp} were always larger than the corresponding sizes estimated from $\sigma_{xy,i}$ at the same u_0, ranging from 2 to 6 cm. In our experiments, the bubble sizes could be roughly estimated by visual observation. Although there were occasional large bubbles of $\sim$10 cm diameter, most bubbles observed in the bed were small, usually in the range of 2–4 cm in diameter, as shown by the band of shading in Figure 5. Therefore, bubble sizes estimated from $\sigma_{xy,i}$ were closer to the actual bubble sizes. The larger bubble size estimated from σ_{dp} may largely arise, as discussed earlier, from the superposition of the bubble-related-wave components of two AP signals, and some compression wave component remaining in the DP fluctuations.

Comparison of power spectral densities

Figure 6 compares the PSDs of AP signals, IOPs, and DP signals at different superficial gas velocities. For PSDs of AP signals, the high-intensity components were concentrated in the range of 0–3 Hz. When superficial gas velocities were low, the highest intensities usually appeared at frequencies near 1 Hz, near the natural oscillation frequency of the fluidized bed.[16–19] This indicates that these components may correspond to the pressure waves caused by oscillation of fluidized particles. At higher superficial gas velocities in our results [PSD(P1)], a high-intensity peak gradually emerged near 0 Hz, as seen most clearly in Figures 6e, f. This component should be related to compression waves generated by gas flow rate fluctuations characterized by very low frequency and increasing amplitude with increasing superficial gas velocity. The above two types of high-intensity components (near 1 and 0 Hz) are both global compression waves. On the other hand, the intensity of compression waves generated by oscillation of fluidized particles (at $f = 1$ Hz) first increased with increasing superficial gas velocity and then began to decrease at $u_0 = 0.37$ m/s, near the onset of the

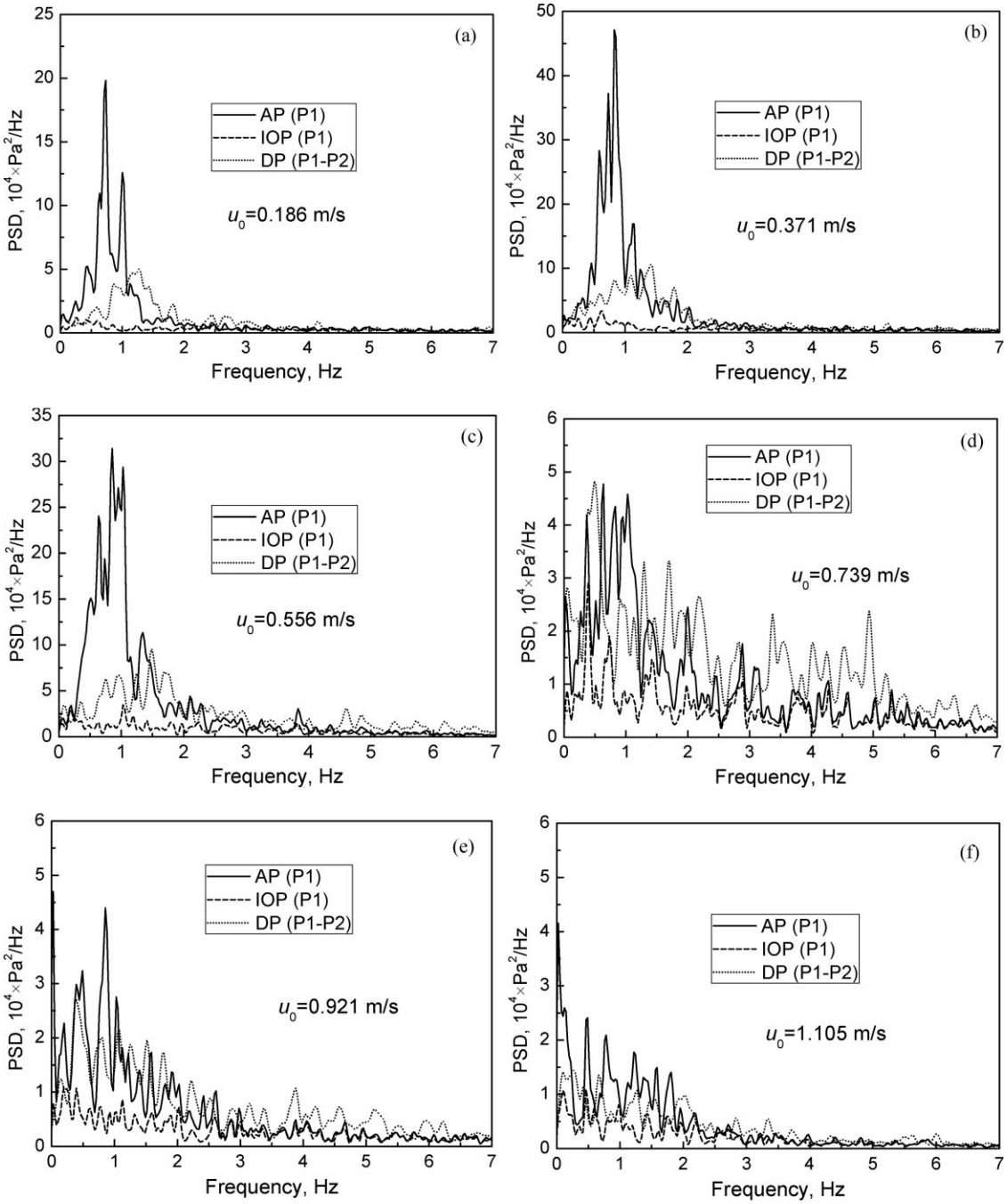

Figure 6. Comparison of power spectral densities of absolute pressure signals, IOPs and differential pressure signals.

turbulent flow regime. The first stage of increasing amplitudes arises mainly from the increase of average bubble size, resulting in stronger energy input and higher intensities. However, bubbles become small transient voids, continuously splitting and coalescing after the turbulent flow regime is reached. The intensities of compression waves generated by oscillation of fluidized particles decrease drastically because of less energy input and stronger attenuation caused by the presence of numerous voids in the bed.

The PSDs of DP signals [PSD(P_1-P_2) in Figure 6] were more evenly distributed across the frequency range. Components at $f = 1$ Hz, generated from oscillation of fluidized particles, were most seriously filtered out by the DP transducer. This can be observed most clearly at low superficial gas velocities, as shown in Figures 6a–c. As u_0 increased, the high-intensity peaks at $f = 0$ Hz, corresponding to the components generated by gas flow rate fluctuations, also attenuated strongly, as can be seen in Figures 6e, f. However, the intensities of the components of DP signals in other frequency ranges were comparable to, or even larger than, those for the AP signals. As bubbles in fluidized beds of fine FCC particles are relatively small, these components likely

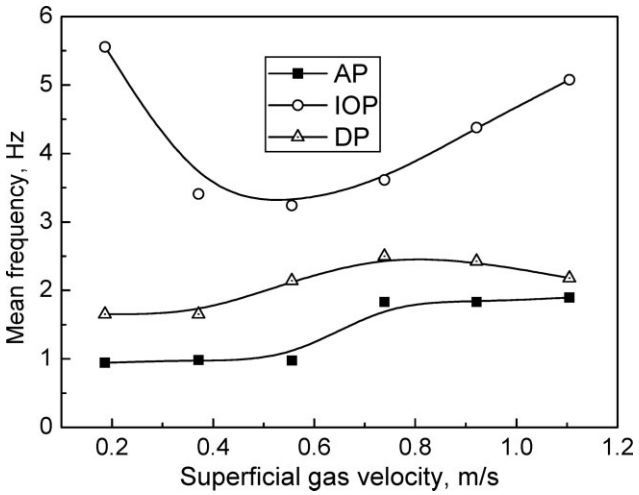

Figure 7. Comparison of mean frequencies of absolute pressure signals, IOPs, and differential pressure signals.

correspond to local bubble behavior, such as passage, breaking, or coalescence. As discussed earlier, these components measured by a DP transducer are less correlated, so they may be superposed in the DP signals.

The PSDs of IOP had the most evenly distributed intensities over the frequency range of interest. Pressure waves generated from the oscillation of fluidized particles (f = 1 Hz) were again filtered most effectively. Similarly, pressure waves generated from gas flow rate fluctuations (f = 0 Hz) were also strongly removed at high superficial gas velocities. On the contrary, components corresponding to bubble behavior or local gas turbulence were mostly retained.

In summary, both IOP and DP fluctuations can significantly filter out the most dominant compression waves in fluidized beds, while retaining more bubble-related local pressure wave components. Therefore, they are more suitable than AP fluctuations for the characterization of bubble behavior in fluidized beds. However, the distance between our two pressure taps of the DP transducer, 0.2 m, a common spacing industrially, was not small enough to remove all compression wave components from the DP signals.

Comparison of mean frequency

The global filtering of different pressure wave components can be characterized by the mean frequency introduced by Trnka et al.,[20] f_m, which satisfies

$$\int_{f_{min}}^{f_m} \phi_{yy}(f)df = \int_{f_m}^{f_{max}} \phi_{yy}(f)df \tag{5}$$

based on the PSD, where f_{min} and f_{max} are the minimum and maximum sampling frequencies. Unlike the dominant frequency, which corresponds to the frequency with the highest amplitude, the mean frequency accounts for all contributions of waves based on their amplitudes, and it is therefore more representative and more reproducible.

Figure 7 compares the mean frequencies of AP signals, IOPs, and DP signals as a function of superficial gas velocity. The mean frequency of the AP was always lowest of the three, because the high-intensity components of AP, i.e., generated from oscillation of fluidized particles or gas flow rate fluctuations, were all in the low frequency range. The mean frequency of AP fluctuations increased monotonously with increasing superficial gas velocity, mainly due to the increasing attenuation of compression wave components generated from oscillation of fluidized particles with increasing superficial gas velocity, as seen in Figure 6. The mean frequency of DP fluctuations had a higher value. This demonstrates that: (1) a large part of low-frequency compression wave components, especially those generated from oscillation of fluidized particles or gas flow rate fluctuations, were filtered out; (2) a large portion of compression waves were still retained in the DP signals. The mean frequency of IOP was highest for all operating conditions investigated, demonstrating that more low-frequency compression wave components were filtered out than for the DP signals.

Comparison of coherence functions

Figure 8 presents the (P_0–P_1) and (P_1–P_2) coherence function curves in the 0–7 Hz frequency range at different superficial gas velocities. As can be seen from Figure 8, there were two main peaks for most operating conditions, representing two main parts of wave component most filtered by the IOP method. One was located at ~1 Hz, corresponding to pressure waves generated from oscillation of fluidized particles and usually dominant at low gas velocities. The other, near 0 Hz, corresponded to pressure waves generated from gas flow rate fluctuations and this one becomes more dominant with increasing superficial gas velocity. The two coherence function curves showed similar trends under most operating conditions, but the coherence function between pressure taps P_1 and P_2 was always lower than that between taps P_0 and P_1. This is because the P_0 pressure signal contained mainly compression wave components, whereas P_1 and P_2 reflected both global compression waves and local bubble-related waves, making these two P_1 and P_2 signals less correlated, resulting in reduced coherence between them. Another reason may be that the axial distance between P_0 and P_1 is larger than between P_1 and P_2, thus making the signals from P_0 and P_1 more correlated.

Comparison of filtering effect

An average coherence in the frequency range of 0–10 Hz between P_0 and P_1,

$$\overline{\gamma_{xy}^2} = \frac{1}{10}\int_0^{10} \gamma_{xy}^2 df, \tag{6}$$

as proposed by Cai et al.,[21] was explored next to quantify the extent of similarity between two AP signals. The larger the average coherence, the more components in the AP signal are filtered out by the IOP method. This average coherence can be viewed as a metric to characterize the extent of filtering by the IOP method.

Another filtering index, based on the absolute deviation,

$$\delta_p = \frac{\sum_1^n |p_i - \bar{p}|}{n}, \tag{7}$$

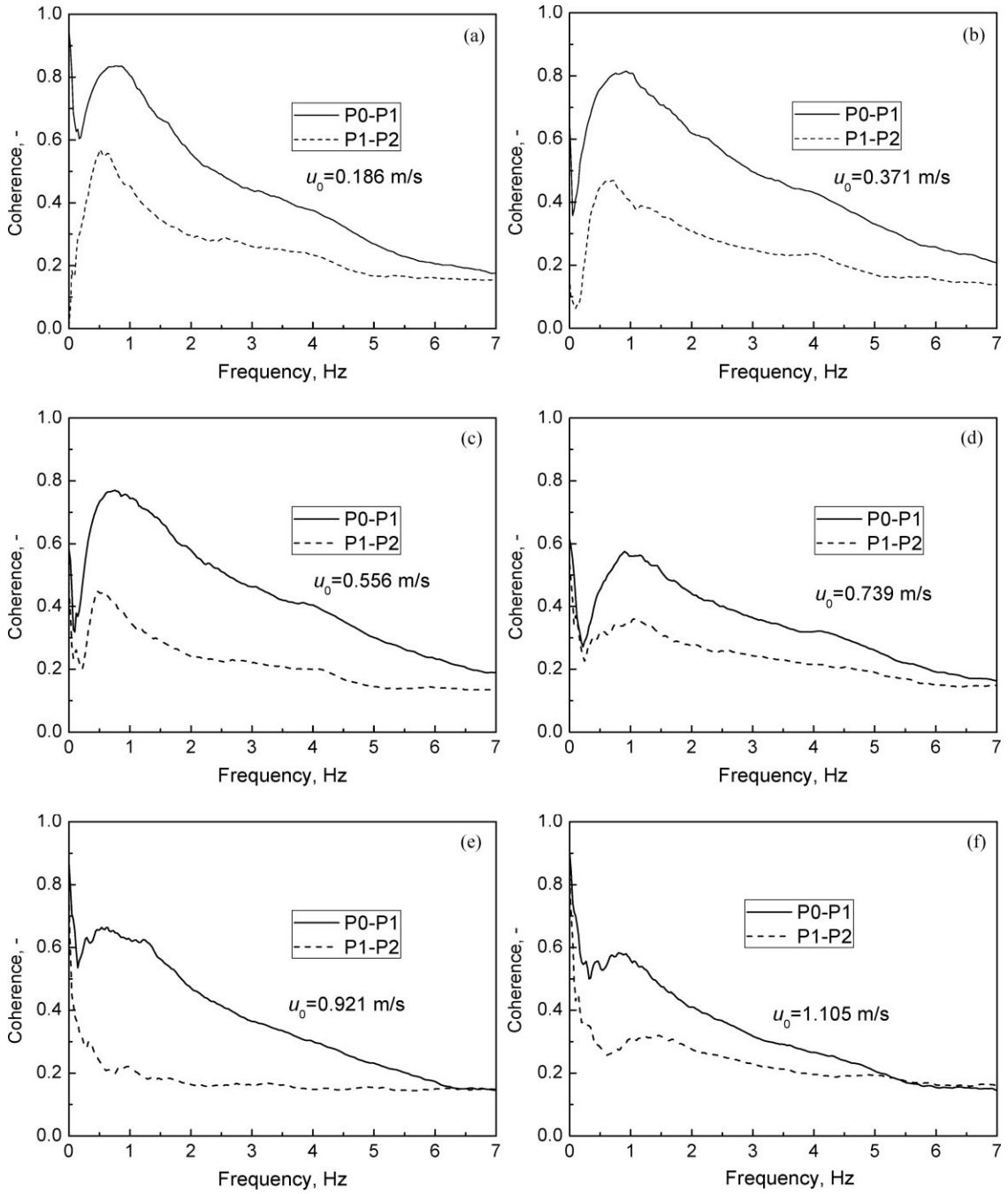

Figure 8. Coherence functions between two in-bed pressure signals (P_1–P_2) and between one in-bed signal and the plenum chamber pressure signal (P_0–P_1).

was also investigated to quantify the extent of filtering by a DP signal. The DP signal is a combination of two AP signals, so the absolute deviation of a DP signal can be written as

$$\delta_{\mathrm{dp}} = \frac{\sum_1^n \left| (p_{1\mathrm{i}} - p_{2\mathrm{i}}) - \overline{(p_1 - p_2)} \right|}{n} = \frac{\sum_1^n |(p_{1\mathrm{i}} - \overline{p_1}) - (p_{2\mathrm{i}} - \overline{p_2})|}{n}. \quad (8)$$

Because of

$$|(p_{1\mathrm{i}} - \overline{p_1}) - (p_{2\mathrm{i}} - \overline{p_2})| \le |(p_{1\mathrm{i}} - \overline{p_1}) + (p_{2\mathrm{i}} - \overline{p_2})|, \quad (9)$$

$$\delta_{\mathrm{dp}} \le \delta_{\mathrm{p1}} + \delta_{\mathrm{p2}}, \quad (10)$$

where δ_{p1} and δ_{p2} are the absolute deviations of the AP signals at the two taps of a DP transducer. A filtering index of DP is defined as

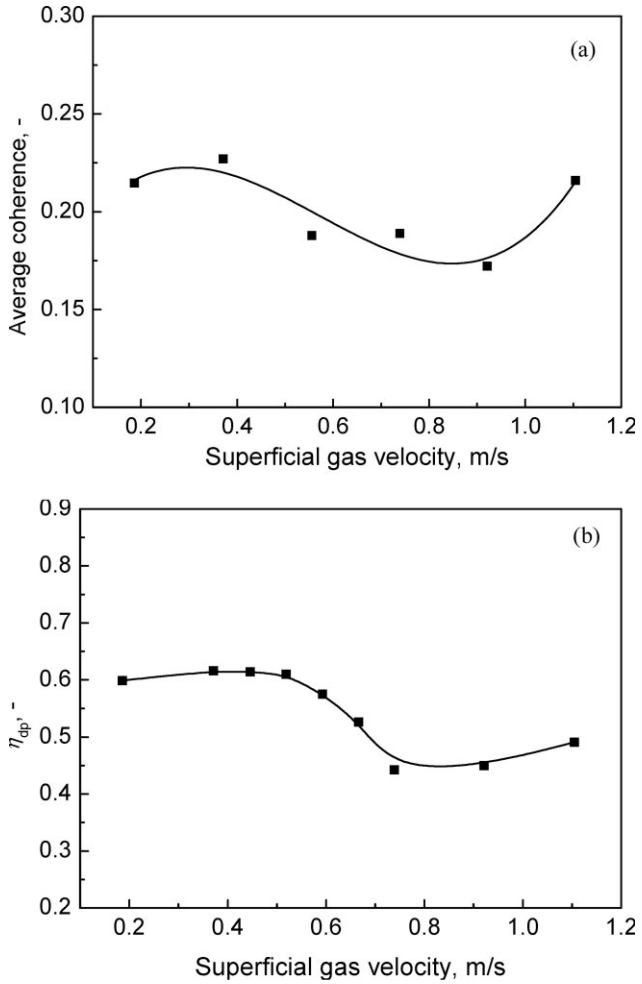

Figure 9. Comparison of (a) average coherence and (b) filtering index of differential pressure.

$$\eta_{dp} = 1 - \frac{\delta_{dp}}{\delta_{p1} + \delta_{p2}}, \tag{11}$$

where $\delta_{p1} + \delta_{p2}$ is the maximum possible absolute deviation of a DP signal. The larger the η_{dp}, the more components of AP signals are filtered out by the DP signal.

Figure 9 shows that the average coherence and η_{dp} followed similar trends with increasing superficial gas velocity: first increasing slightly and then decreasing as the superficial gas velocity increased. For $u_0 > \sim 0.8$ m/s, both indices increased again. The results again demonstrated their similar effect on the filtering of pressure waves.

In summary, the above comparisons confirm the similar filtering effects of IOP and DP fluctuations. It is also clear that both methods are imperfect. Some compression wave components may still remain in IOP and DP fluctuations, whereas some useful bubble-related wave components tend to be filtered out by both methods. If the distance between two pressure taps of a DP transducer is appropriately chosen, the amplitude of DP fluctuations can be as useful as the IOP amplitude in characterizing the average bubble size and the quality of gas–solids contacting. However, bubble sizes derived from their amplitudes, e.g., by Eq. 4, are at best approximate because of the difficulties in filtering out all compression wave components and retaining all useful and uncorrelated wave components.

Conclusions

In this study, the two common decoupling methods for the analysis of pressure fluctuations in fluidized beds, i.e., IOP and DP fluctuations, are analyzed and evaluated based on their amplitudes, power spectral densities, mean frequencies, coherence functions, and two filtering indices. It can be concluded that:

(1) Both IOP and DP fluctuations can significantly filter out global compression wave components, especially those generated from oscillations of fluidized particles and gas flow rate fluctuations.

(2) Both methods are imperfect. They neither filter out all compression wave components nor retain all useful bubble-related wave components.

(3) Both the amplitudes of IOP and DP fluctuations can be used to characterize global bubble properties and the quality of gas–solids contacting, but neither is able to provide accurate bubble sizes.

(4) For DP fluctuations to optimally characterize bubble properties, the distance between adjacent pressure taps of the DP transducer should be small enough to filter out more compression wave components, but larger than half the average bubble diameter to avoid excessive removal of bubble-related wave components.

Acknowledgments

The authors acknowledge the financial support from the National Natural Science Foundation of China for Distinguished Young Scholars of China (Grant No. 20525621), the National Basic Research Program of China (Grant No. 2004CB217801), and the Chinese Scholarship Council.

Notation

d_b = bubble diameter, m
d_p = particle diameter, m
d_t = column diameter, m
f = frequency, Hz
f_m = mean frequency, Hz
f_{min}, f_{max} = minimum and maximum sampling frequencies, Hz
g = gravitational acceleration, m/s
H_{mf} = bed height at minimum fluidization velocity, m
IOP, COP = incoherent and coherent parts of power spectral density of absolute pressure in the bed with respect to the plenum chamber pressure signal, Pa^2/Hz
n = number of sampling data points
p_i = transient pressure value, Pa
P_0 = absolute pressure in chamber, Pa
P_1, P_2 = absolute pressure at taps 1 and 2 in bed, Pa
u_b = bubble rise velocity, m/s
u_0 = superficial gas velocity, m/s

Greek letters

δ_p, δ_{dp} = absolute deviations of absolute and differential pressure signals, Pa
ε_{mf} = voidage at minimum fluidization
ϕ_{xx}, ϕ_{yy} = power spectral density, Pa^2/Hz
ϕ_{xy} = cross-power spectral density, Pa^2/Hz
γ^2_{xy} = coherence function
$\overline{\gamma^2_{xy}}$ = average coherence function between 0 and 10 Hz

η_{dp} = filtering index of differential pressure signal
ρ_p = particle density, kg/m^3
σ_{dp}, σ_p = standard deviations of differential and absolute pressure fluctuations, Pa
$\sigma_{xy,i}$, $\sigma_{xy,c}$ = standard deviations of incoherent and coherent parts of absolute pressure fluctuations, Pa

Literature Cited

1. van Ommen JR, Mudde RF. Measuring the gas-solids distribution in fluidized beds—a review. *Int J Chem React Eng*. 2008;6:R3. Available at www.bepress.com/ijcre/vol6/R3/.
2. Bi HT. A critical review of the complex pressure fluctuation phenomenon in gas-solids fluidized beds. *Chem Eng Sci*. 2007;62:3473–3493.
3. Davidson JF. Symposium on fluidization-discussion. *Trans Inst Chem Eng*. 1961;39:230–232.
4. van der Schaaf J, Schouten IC, Johnsson F, van den Bleek CM. Non-intrusive determination of bubble and slug length scales in fluidized beds by decomposition of the power spectral density of pressure time series. *Int J Multiphase Flow*. 2002;28:865–880.
5. Darton RC, Lanauze RD, Davidson JF, Harrison D. Bubble growth due to coalescence in fluidized beds. *Trans Inst Chem Eng*. 1977;55:274–280.
6. Kleijn van Willigen F, van Ommen JR, van Turnhout J, van den Bleek CM. Bubble size reduction in a fluidized bed by electric fields. *Int J Chem React Eng*. 2003;1:A21. Available at: http://www.bepress.com/ijcre/vol1/A21.
7. Roy R, Davidson JF. *Similarity between gas-fluidized beds at elevated temperature and pressure*. In: Grace JR, Shemilt LW, Bergougnou MA, editors. *Fluidization VI*. New York: AIChE, 1989:293–300.
8. Bi HT. Flow Regime Transitions in Gas-Solids Fluidization and Transport. Doctoral dissertation, University of British Columbia, Vancouver, Canada, 1994.
9. Bi HT, Grace JR, Zhu JX. Propagation of pressure wave and forced oscillations in gas-solid fluidized beds and their influence on diagnostics of local hydrodynamics. *Powder Technol*. 1995;82:239–253.
10. Musmarra D, Poletto M, Vaccaro S, Clift R. Dynamic wave in fluidized beds. *Powder Technol*. 1995;8:255–268.
11. Cai P, Miu Z, Yu ZQ, Jin Y. Mathematic features and analyzing methods of pressure fluctuation signal from a gas-solid fluidized bed. *Eng Chem Metall*. 1990;11:114–122 (in Chinese).
12. Mori S, Wen CY. Estimation of bubble diameter in gaseous fluidized beds. *AIChE J*. 1975;21:109–115.
13. Horio M, Nonaka A. A generalized bubble diameter correlation for gas-solid fluidized beds. *AIChE J*. 1987;33:1865–1872.
14. Choi JH, Son JE, Kim SD. Generalized model for bubble size and frequency in gas-fluidized beds. *Ind Eng Chem Res*. 1998;37:2559–2564.
15. Clark NN, Atkinson CM. Amplitude reduction and phase lag in fluidized-bed pressure measurements. *Chem Eng Sci*. 1988;43:1547–1557.
16. Verloop J, Heertjes PM. Periodic pressure fluctuations in fluidized beds. *Chem Eng Sci*. 1974;29:1035–1042.
17. Baskakov AP, Tuponogov VG, Filippovsky NF. A study of pressure fluctuations in a bubbling fluidized bed. *Powder Technol*. 1986;45:113–117.
18. Hao BG, Bi HT. Forced bed mass oscillations in gas-solid fluidized beds. *Powder Technol*. 2005;149:51–61.
19. Sasic S, Leckner B, Johnsson F. Time-frequency investigation of different modes of bubble flow in a gas-solid fluidized bed. *Chem Eng J*. 2006;121:27–35.
20. Trnka O, Vesely V, Hartman M. Identification of the state of a fluidized bed by pressure fluctuations. *AIChE J*. 2000;46:509–514.
21. Cai P, Jin Y, Yu ZQ, Wang ZW. Mechanism of flow regime transition from bubbling to turbulent fluidization. *AIChE J*. 1990;36:955–956.

Manuscript received Jan. 12, 2009, and revision received May 29, 2009.